# Thermal and optical properties of the femtosecond-laser-structured and stress-induced birefringent regions in sapphire

**Junko Morikawa**[1,3], **Akihiro Orie**[1], **Toshimasa Hashimoto**[1], **Saulius Juodkazis**[2,*]

[1] *Tokyo Institute of Technology, Meguro-ku, Tokyo 152-8550, Japan*

[2] *Centre for Micro-Photonics, Faculty of Engineering and Industrial Sciences Swinburne University of Technology, Hawthorn, VIC, 3122, Australia*
[3]*morikawa.j.aa@m.titech.ac.jp (JM)*
[*]*sjuodkazis@swin.edu.au (SJ)*

**Abstract:** Temperature diffusivity of laser micro-structured regions in sapphire is determined by a temperature wave method with a lateral resolution reduced to $\sim 10\ \mu$m using a directly sputtered micro-sensor and heater. A record high reduction of the temperature diffusivity of sapphire by 12% from its $(1.26 \pm 0.02) \times 10^{-5}$ m$^2$/s in-bulk value inside the femtosecond laser-structured volumes is determined; in a BK7 glass ($\sim 4.8 \times 10^{-7}$ m$^2$/s), a 2% decrease of the thermal diffusivity has been observed. Origin of the reduction is consistent with disorder and scattering of phonons around the laser photo-modified micro-volumes. The stress-induced birefringence is directly measured by polariscopy together with its radial distribution, and azimuthal orientation of the polarization ellipsis near the laser structured regions in sapphire. The maximum birefringence of $\Delta n \simeq 1 \times 10^{-3}$ is achieved without crack formation and corresponds to a local stress of $\sim 1.3$ GPa. The stress (and birefringence) decay radially with a single-exponential constant of $\tau_R = 24\ \mu$m while the azimuthal orientation of the polarization ellipsis is spiraling around the laser structured volume. Such structures are promising in waveguiding and lasing applications of optical vortices where spatial control of birefringence and optical activity are required.



**OCIS codes:** (140.3390) Laser materials processing; (220.4000) Microstructure fabrication; (160.1585) Chiral media; (60.1245) Artificially engineered materials.

## References and links

1. M. Ams, G. D. Marshall, P. Dekker, J. A. Piper, and M. J. Withford, "Ultrafast laser written active devices," Laser Photon. Rev. **3**, 535–544 (2009).
2. S. K. Sundaram and E. Mazur, "Inducing and probing non-thermal transitions in semiconductors using femtosecond laser pulses," Nature Mat. **1**, 217–224 (2002).
3. Y. Lan, A. J. Minnich, G. Chen, and Z. Ren, "Enhancement of thermoelectric figure-of-merit by a bulk nanostructuring approach," Adv. Func. Mat., **20**, 357–376 (2010).
4. S. Juodkazis, V. Mizeikis, and H. Misawa, "Three-dimensional microfabrication of materials by femtosecond lasers for photonics applications," J. Appl. Phys. **106**, 051101 (2009).

#123699 - $15.00 USD Received 2 Feb 2010; revised 26 Mar 2010; accepted 29 Mar 2010; published 6 Apr 2010

5. S.Sowa, W. Watanabe, T.Tamaki, J. Nishii, and K. Itoh, "Symmetric waveguides in poly(methyl methacrylate) fabricated by femtosecond laser pulses," Opt. Express **14**, 291–297 (2006).
6. S. Nolte, M. Will, J. Burghoff, and A. Tünnermann, "Femtosecond waveguide writing: a new avenue to three-dimensional integrated optics," Appl. Phys. A **77**, 109–111 (2003).
7. L. Shah, A. Arai, S. Eaton, and P. Herman, "Waveguide writing in fused silica with a femtosecond fiber laser at 522 nm and 1 MHz repetition rate," Opt. Express **13**, 1999–2006 (2005).
8. D. M. Krol, "Femtosecond laser modification of glass," J. Non-Cryst. Sol. **354**, 416–424 (2009).
9. G. Cerullo, R. Osellame, S. Taccheo, M. Marangoni, D. Polli, R. Ramponi, P. Laporta, and S. D. Silvestri, "Femtosecond micromachining of symmetric waveguides at 1.5$\mu$m by astigmatic beam focusing," Opt. Lett. **27**, 1938–1940 (2002).
10. J. Siebenmorgen, K. Petermann, G. Huber, K. Rademaker, and S. N. A.Tünnermann, "Femtosecond laser written stress-induced Nd:$Y_3Al_5O_{12}$(Nd:YAG) channel waveguide laser," Appl. Phys. B **97**, 251–255 (2009).
11. A. Benayas, D. Jaque, B. McMillen, and K. P. Chen, "High repetition rate UV ultrafast laser inscription of buried channel waveguides in sapphire: Fabrication and fluorescence imaging via ruby R lines," Opt. Express **17**, 10076–10081 (2009).
12. Z. Zhu and T. G. Brown, "Stress-induced birefringence in microstructured optical fibers," Opt. Lett. **28**, 2306–2308 (2003).
13. G. Cheng, K. Mishchik, C. Mauclair, E. Audouard, and R. Stoian, "Ultrafast laser photoinscription of polarization sensitive devices in bulk silica glass," Opt. Express **17**, 9515–9525 (2009).
14. J. Siebenmorgen, T. Calmano, O. Hellmig, K. Petermann, and G. Huber, "Efficient femtosecond laser written Nd:YAG channel waveguide laser with an output power of more than 1 W,", Technical Digest, CLEO/Europe-EQEC Conference, 2009, paper CJ7.1.
15. J. Morikawa, C. Leong, T. Hashimoto, T. Ogawa, Y. Urata, S. Wada, M. Higuchi, and J.-I. Takahashi, "Thermal conductivity/diffusivity of $Nd^{3+}$ doped $GdVO_4$, $YVO_4$, $LuVO_4$,and $Y_3Al_5O_{12}$ by temperature wave analysis," J. Appl. Phys. **103**, 063522 (2008).
16. S. M. Eaton, H. Zhang, M. L. Ng, J. Z. Li, W. J.Chen, S. Ho, and P. R. Herman, "Transition from thermal diffusion to heat accumulation in high repetition rate femtosecond laser writing of buried optical waveguides," Opt. Express **16**, 9443–9458 (2008).
17. J. Morikawa and T. Hashimoto, "Thermal diffusivity of aromatic polyimide thin films by temperature wave analysis," J. Appl. Phys. **105**, 113506 (2009).
18. Y. Bellouard, M. Dugan, A. A. Said, and P. Bado, "Thermal conductivity contrast measurement of fused silica exposed to low-energy femtosecond laser pulses," Appl. Phys. Lett. **89**, 161911 (2006).
19. T. Hashimoto, S. Juodkazis, and H. Misawa, "Void recording in silica," Appl. Phys. A **83**, 337–340 (2006).
20. A. Marcinkevicius, V. Mizeikis, S. Juodkazis, S. Matsuo, and H. Misawa, "Effect of refractive index-mismatch on laser microfabrication in silica glass," Appl. Phys. A. **76**, 257–260 (2003).
21. E. E. Gamaly, S. Juodkazis, K. Nishimura, H. Misawa, B. Luther-Davies, L. Hallo, P. Nicolai, and V. Tikhonchuk, "Laser-matter interaction in a bulk of a transparent solid: confined micro-explosion and void formation," Phys. Rev. B **73**, 214101 (2006).
22. M. Shribak and R. Oldenbourg, "Techniques for fast and sensitive measurements of two-dimensional birefringence distributions," Appl. Opt. **42**, 3009–3017 (2003).
23. E. Vanagas, I. Kudryashov, D. Tuzhilin, S. Juodkazis, S. Matsuo, and H. Misawa, "Surface nanostructuring of borosilicate glass by femtosecond nJ energy pulses," Appl. Phys. Lett. **82**, 2901–2903 (2003).
24. S. Juodkazis, K. Yamasaki, V. Mizeikis, S. Matsuo, and H. Misawa, "Formation of embedded patterns in glasses using femtosecond irradiation," Appl. Phys. A **79**, 1549–1553 (2004).
25. S. Juodkazis, K. Nishimura, H. Misawa, T. Ebisui, R. Waki, S. Matsuo, and T. Okada, "Control over the state of crystallinity: Sapphire," Adv. Mat. **18**, 1361–1364 (2006).
26. S. Juodkazis, K. Nishimura, S. Tanaka, H. Misawa, E. E. Gamaly, B. Luther-Davies, L. Hallo, P. Nicolai, and V. Tikhonchuk, "Laser-induced microexplosion confined in the bulk of a sapphire crystal: Evidence of multi-megabar pressures," Phys. Rev. Lett. **96**, 166101 (2006).
27. J. Morikawa, A. Orie, T. Hashimoto, and S. Juodkazis, "Thermal diffusivity in femtosecond-laser-structured micro-volumes of polymers," Appl. Phys. A. **98**, 551–556 (2010).
28. B. Rogers, S. Pennathur, and J. Adams, *Nanotechnology: understanding small systems* (CRC Press Taylor and Francis Group, Boca Raton, 2008).
29. K. Ueno, S. Juodkazis, T. Shibuya, V. Mizeikis, Y. Yokota, and H. Misawa, "Nano-particle-enhanced photopolymerization," J. Phys. Chem. C **113**, 11720–11724 (2009).
30. M. J. Assael, K. D. Antoniadis, and J. Wu, "New measurements of the thermal conductivity of PMMA, BK7, and Pyrex 7740 up to 450K," Int. J. Thermophys. **292**, 1257–1266 (2008).
31. Y. Bellouard, T. Colomb, C. Depeursinge, M. Dugan, A. A. Said, and P. Bado, "Nanoindentation and birefringence measurements on fused silica specimen exposed to low-energy femtosecond pulses," Opt. Express **14**, 8360–8366 (2006).
32. H. Aben, *Photoelasticity of glass* (Springer-Verlag Berlin, 1993).
33. E. Brasselet, N. Murazawa, H. Misawa, and S. Juodkazis, "Optical vortices from liquid crystal droplets," Phys.

#123699 - $15.00 USD Received 2 Feb 2010; revised 26 Mar 2010; accepted 29 Mar 2010; published 6 Apr 2010

Rev. Lett. **103**, 103903 (2009).
34. V. Mizeikis, S. Kimura, N. V. Surovtsev, V. Jarutis, A. Saito, H. Misawa, and S.Juodkazis, "Formation of amorphous sapphire by a femtosecond-pulse-induced micro-explosion," Appl. Surf. Sci. **255**, 9745 – 9749 (2009).
35. L. Allen, M. J. Padgett, and M. Babiker, "The orbital angular momentum of light," Progress in Optics **39**, 291–372 (1999).
36. M. Berry, "Making waves in physics," Nature **403**, 21 (2000).
37. K. T. Gahagan and G. A. Swartzlander, "Optical vortex trapping of particles," Opt. Lett. **21**, 827–829 (1996).
38. M. Harris, C. A. Hill, P. R. Tapster, and J. M. Vaughan, "Laser modes with helical wave fronts," Phys. Rev. A **49**, 3119–3122 (1994).
39. G. Foo, D. M. Palacios, and G. A. Swartzlander, "Optical vortex coronagraph," Opt. Lett. **30**, 3308–3310 (2005).
40. H. He, M. E. J. Friese, N. R. Heckenberg, and H. Rubinsztein-Dunlop, "Direct observation of transfer of angular-momentum to absorptive particles from a laser-beam with a phase singularity," Phys. Rev. Lett. **75**, 826–829 (1995).
41. P. G. Eliseev, S. Juodkazis, T. Sugahara, H.-B. Sun, S. Matsuo, S. Sakai, and H. Misawa, "GaN surface ablation by fs-pulses: atomic force microscopy studies, accumulation effects," in Proceedings of *High-Power Laser Ablation Conf.* (SPIE Proc. **4065**, 2000) pp.546–556.
42. R. A. L. Jones, *Soft Condensed Matter* (Oxford University Press, 2002).
43. A. K. Spilman and T. G. Brown, "Stress birefringent, space-variant wave plates for vortex illumination," Appl. Optics **46**, 61-66 (2007).
44. M. E. J. Friese, T. A. Nieminen, N. R. Heckenberg, and H. Rubinsztein-Dunlop, "Optical alignment and spinning of laser-trapped microscopic particles," Nature **394**, 348–350 (1998).
45. S. Juodkazis, M. Shikata, T. Takahashi, S. Matsuo, and H. Misawa, "Fast optical swithing by a laser manipulated microdroplet of liquid crystal," Appl. Phys. Lett. **74**, 3627–3629 (1999).
46. S. Juodkazis, S. Matsuo, N. Murazawa, I. Hasegawa, and H. Misawa, "High-efficiency optical transfer of torque to a nematic liquid crystal," Appl. Phys. Lett. **82**, 4657–4659 (2003).
47. E. Brasselet, Y. Izdebskaya, V. Shvedov, A. S. Desyatnikov, W. Krolikowski, and Y. S. Kivshar, "Dynamics of optical spin-orbit coupling in uniaxial crystals," Opt. Lett. **34**, 1021–1023 (2009).
48. A. Ciattoni, G. Cincotti, and C. Palma, "Angular momentum dynamics of a paraxial beam in a uniaxial crystal," Phys. Rev. E **67**, 036618 (2003).
49. L. Marrucci, C.Manzo, and D. Paparo, "Optical spin-to-orbital angular momentum conversion in inhomogeneous anisotropic media," Phys. Rev. Lett. **96**, 163905 (2006).
50. N. B. Simpson, K. Dholakia, L. Allen, and M. J. Padgett, "Mechanical equivalence of spin and orbital angular momentum of light: An optical spanner," Opt. Lett. **22**, 52–54 (1997).
51. H. Misawa and S. Juodkazis, "Photophysics and photochemistry of a laser manipulated microparticle," Prog. Polym. Sci. **24**, 665–697 (1999).
52. P. A. Williams, A. H. Rose, K. S. Lee, D. C. Conrad, G. W. Day, and P. D. Hale, "Optical, thermo-optic, electro-optic, and photoelastic properties of bismuth germanate $ABi_4Ge_3O_{12}B$," Appl. Opt. **35**, 3562 – 3569 (1996).
53. "http://en.wikipedia.org/wiki/Hooke's_law."
54. J. W. Kysar, "Path of light in near crack tip region in anisotropic medium and under mixed-mode loading," Int. J. Sol. Struct. **38**, 5963–5973 (2001).
55. J. Reintjes and M. B. Schulz, "Photoelastic constants of selected ultrasonic delay-line crystals," J. Appl. Phys. **39**, 5254 – 5258 (1968).
56. J. M. Winey, Y. M. Gupta, and D. E. Hare, "r-axis sound speed and elastic properties of sapphire single crystals," J. Appl. Phys. **90**, 3109 – 3111 (2001).
57. T. A. Davis and K. Vedam, "Photoelastic properties of sapphire ($\alpha$ - $Al_2O_3$)," J. Appl. Phys. **38**, 4556 – 4557 (1967).
58. M. Beresna, T. Gertus, R. Tomasiunas, H. Misawa, and S. Juodkazis, "Three-dimensional modeling of the heat-affected zone in laser machining applications," Laser Chemistry **2008**, 976205 (2008).
59. K. Syassen, "Ruby under pressure," High Pressure Research **28**, 75–126 (2008).

## 1. Introduction

Thermal, mechanical, and optical properties of materials are strongly interrelated and by controlling structural changes on a sub-wavelength scale inside optical materials their mechanical, thermo-electrical, and optical behavior [1–4], relevant to an increasing number of applications in the fields of micro-optics, lab-on-a-chip, optofluidics, waveguiding, and lasing should be better understood. Waveguides directly recorded by laser beam inside plastics [5], optically active and passive glasses [6–9] and crystals [10, 11] are used for sensing, beam splitting/multiplexing, and lasing applications. Birefringent regions formed alongside the laser-recorded micro-structures can also support waveguiding [12, 13]. Recently, a high 1 W output

#123699 - $15.00 USD Received 2 Feb 2010; revised 26 Mar 2010; accepted 29 Mar 2010; published 6 Apr 2010

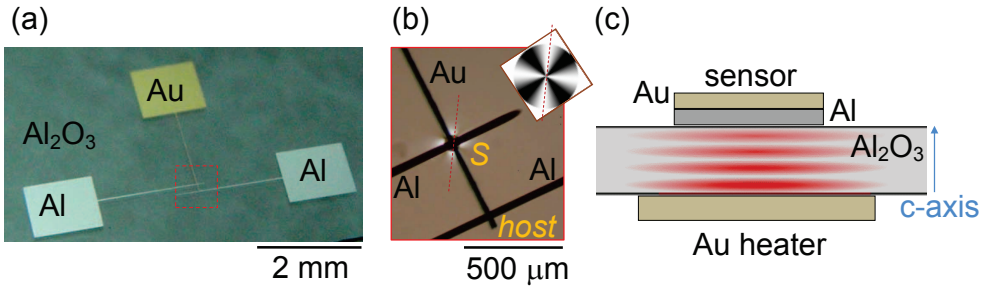


Fig. 1. (a) $Al_2O_3$ wafer padded with sputtered Au and Al electrodes used for thermal diffusivity measurements with a close up polariscope view (b) of the laser-structured volume. The sensor *(S)* and reference *(host)* positions are marked, respectively. Inset in (b) shows simulated transmission profile according to eqn. 3; the transmission pattern is orientated in the same way as in actual experiments. (c) Schematics of the thermal wave propagation from the heater (on bottom) towards the hot-junction sensor (on top); not to scale. See, the experimental section for details.

power with good mode quality and 60% conversion efficiency from laser structures in YAG has been reported [14], where the emission is guided in the birefringent region between two inscribed planes inside Nd:YAG crystal.

For future micro-lasing applications thermal properties of laser crystals and glasses should be well controlled since they are critically important for the long term stability of active micro-optical devices. The thermal properties are dependent on the dopant and defect concentration [15] which affect formation of thermal lensing and might be detrimental for laser operation, especially, at high output power. In the case of the laser inscribed waveguides, the local redistribution of the dopants, laser-induced defects, and even changes of local mass density are all taking place and influence optical functions [16]. A direct measurement of the thermal properties is the required approach [15,17], however, there is lack of techniques allowing direct quantitative measurement of thermal conductivity and diffusivity with a high $<$1% precision on a micrometer scale. Atomic force microscopy can be used to detect the relative change of thermal properties on a micrometer scale [18], however it is difficult to make such measurement quantitative. The most challenging issue is miniaturization of sensors and thermal contact with sample.

Here, we report on direct measurement of thermal diffusivity by a miniaturized temperature wave (TW) method applied for a high-fidelity characterization of the micro-volumes inside laser-structured sapphire. A record high, up to 12% reduction of thermal diffusivity has been observed in laser structured volumes. The regions just adjacent ($\sim 3$ $\mu$m separation) to the ones modified, showed no change of the bulk diffusivity. The stress-induced birefringence near the femtosecond (fs)-laser-structured micro-volumes of tens-of-micrometers in cross section is measured by polariscopy and can amount to $\Delta n \simeq 1 \times 10^{-3}$ suitable for waveguide formation. The stress and birefringence show exponential relaxation over length of 24 $\mu$m (with the maximum stress estimated to reach 1.3 GPa). The Stokes analysis of birefringence revealed a typical $2\pi$ spiraling phase around cylindrical laser-structured volume and could be used for generation of optical vortex.

#123699 - $15.00 USD Received 2 Feb 2010; revised 26 Mar 2010; accepted 29 Mar 2010; published 6 Apr 2010

## 2. Experimental details

Femtosecond laser pulses 150 fs/800 nm were focused inside samples of sapphire and glass using an objective lens of numerical aperture $NA = 1.4$ [19]. The irradiation spots were closely packed with typical separations in lateral (x and y) and axial (z) directions: $2 \times 2 \times 1.5$ $\mu$m. Due to high refractive index of sapphire, $n = 1.7$ at 800 nm wavelength used for laser structuring, the actual axial period between planes was comparable with the lateral period between void-structures. Also, the regions recorded at larger depth ($\sim 100$ $\mu$m) had axially elongated shape due to spherical aberrations [20]. The modified regions were cylindrical with 35 $\mu$m in diameter and 90 $\mu$m in height to maximize the modified volume within a 126 $\mu$m-thick sapphire slab (Shinkoshya Inc.) and BK7 107-$\mu$m-thick glass for comparison. Pulse energy used to form void-structures (void with an amorphous shell) in sapphire was 80–120 nJ/pulse at the focus. At these conditions the void of approximately 300 nm in diameter with the amorphous 300-nm-shell were formed [21]; in BK7 glass, pulse energies were 60–90 nJ.

The TW method used for high sensitivity measurements of thermal properties of laser host materials [15,17] was adopted for the thermal diffusivity measurements. Typical surface roughness of the thermo-sensors is $< 100$ nm (min-max) after polishing with a 0.1-$\mu$m diamond powder. However, such sensor arrays were not suitable for the high precision direct measurements using glass and sapphire with optical grade surfaces due to imperfect thermal contacts at the sensor-sample interface. We sputtered the micro-sensors and heaters for reliable implementation of the TW method which rely on the measurement of the phase delay, $\Delta\theta$, using lock-in technique [15,17]:

$$\Delta\theta = -\sqrt{\frac{\pi f}{\chi}}d - \theta_0, \tag{1}$$

where $\chi$ is the thermal diffusivity, $f$ is the repetition rate of the heat wave generation, $d$ is the thickness of sample, and $\theta_0$ is the phase accounting for actual experimental conditions and background noise (it has no significance for the experimental determination of $\chi$ judged from the slope according to eqn. 1).

The sputtered contacts are chemically stable, have a low electric resistivity and good thermal conductivity: 315 W/mK for Au and 237 W/mK for Al. The thickness of the sputtered Au-Al sensor layer was controlled by monitoring the electric resistance. Typically, sensor of 350-440 $\Omega$ was used which does not add up noise to measurements as compared with a thermal noise, $V = \sqrt{4kTR\Delta f}$, where $k$ is the Boltzmann constant, $R$ is the electrical resistance, and $\Delta f$ is the bandwidth in herz over which the noise is measured. The sensor was wired via a cold junction with a copper lead. The sensor hot-junctions were simultaneously sputtered on the fabricated, non-fabricated, and adjacent to the laser-structures regions. Precision of the placement of the hot-junctions was approximately 1 $\mu$m. Series of up to 10 independent measurements of thermal diffusivity were carried out by chemically removing and resputtering the hot-junction contacts and heater.

A heat source for generation of the temperature wave was a 300-nm-thick layer of Au with an area size of $0.4 \times 1.5$ mm$^2$ and is larger than the sensor Au-Al junction. It has an electric resistance of 30 $\Omega$. The larger area assures the one-dimensional heat flow. The heater was wired with a copper lead and the modulated thermal power was chosen to satisfy a good signal-to-noise ratio required for detection of thermal diffusivity changes on the order of $< 1\%$. The temperature jumps were on the order of a few degrees as confirmed by IR thermography and no any changes of structural defects in the laser structured volume occurred.

Polarimetric Stokes analysis was used to determine the birefringence and its spatial distribution around cylindrical micro-structured volumes in sapphire using Abrio IM (Cambridge Research & Instrumentation, Inc.) microscope at 546 nm wavelength [22]. Setup is based on an

#123699 - $15.00 USD Received 2 Feb 2010; revised 26 Mar 2010; accepted 29 Mar 2010; published 6 Apr 2010

Olympus BX41 microscope equipped with a UPlanFI $40^{\times}$ objective lens of numerical aperture $NA = 1.3$.

## 3. Results and discussion

The *direct laser writing* by tightly focused femtosecond laser pulses [23, 24] was used to fabricate regions of amorphised sapphire inside crystalline sample at the exactly same conditions as in the previous amorphisation studies [21, 25]. All the samples used in this work were irradiated by tightly focused fs-laser pulses at energy-per-pulse larger than the void formation when the irradiated region has a void surrounded by amorphised shell [19, 26]. Such structural modifications were the focus of this study. Irradiation spots were closely packed to maximize the modified volume.

For this study a micro-scale thermoelectric sensor of Au-Al hot-junctions with a $10 \times 10\ \mu\text{m}^2$ footprint was directly sputtered over the laser-structured regions with a heater sputtered on the opposite side as shown in Fig. 1. This made a perfect surface thermal contact otherwise not possible to achieve with a previous sensor arrangement [27] on high-quality optical surfaces. Next, we analyze the interplay of the thermal, mechanical (stress), and optical (birefringence and optical activity) properties of the laser structured sapphire.

### *3.1. Thermal diffusivity in micro-volumes*

Figure 2 shows normalized thermal diffusivity collected from the regions through the laser-structured, adjacent to it, and at unaffected (*host*) regions of sapphire sample. Each measurement was carried out after stripping out and re-deposition of contacts and heaters (Fig. 2(a)). Since every single set of sputtered contacts and heaters has slightly different thickness we present data normalized, i.e., the thermal diffusivity of the region *S* is divided by the value measured at *host* (see, Fig. 1(b)). The absolute value of thermal diffusivity of host sapphire crystal was determined as $(1.28 \pm 0.016) \times 10^{-5}$ m$^2$/s at 39°C. A high up to 12% decrease of the thermal diffusivity was observed through the laser structured region repeatedly in separate measurements with overall uncertainty $\sim 1\%$. Good correspondence of relative changes in thermal diffusivity were observed in repeated measurements. The heat diffusion took place along c-axis (perpendicular to the image plane in Fig. 1(a,b)). Polariscope image show characteristic Maltese cross lobes due to stress-induced birefringence extending laterally up to $\sim 20\ \mu$m from the laser-structured regions without crack initiation (Fig. 2(b)).

The region just adjacent to the laser-structured volume has no measurable decrease of thermal diffusivity (*3* in Fig. 2). This is the region where stress-induced birefringence is the largest and waveguiding can be realized. Having thermal properties not changed in that particular location is a promising feature for waveguiding and especially lasing applications. The relative changes of thermal diffusivity were reliably measured over 10 cycles (Fig. 2(a)) confirming a high fidelity of the used TW method.

The cause of the decrease in thermal diffusivity is the laser-induced amorphisation and structural modifications around the irradiation spots [26]. The pulse energy was above a threshold of void formation and strong structural modifications occurred around the irradiated volume [19,26]. The thermal diffusivity is defined by the thermal conductivity, $k_c$, the mass density, $\rho_m$ and the specific heat $c_p$ at constant pressure as $\chi = k_c/(\rho_m c_p)$ and was directly measured in our experiments. The thermal conductivity, $k_c$, is given by [28]:

$$k_c = \rho c_p \nu \Lambda / 3, \tag{2}$$

where $\nu$ is the mean velocity of the thermal carriers phonons and electrons, $\rho$ is the density of the carriers, and $\Lambda = \nu\tau$ is the mean free path of the carriers defined via the thermal velocity $\nu$ and average time interval between scattering events, $\tau$. When dimensions of objects become

#123699 - $15.00 USD Received 2 Feb 2010; revised 26 Mar 2010; accepted 29 Mar 2010; published 6 Apr 2010

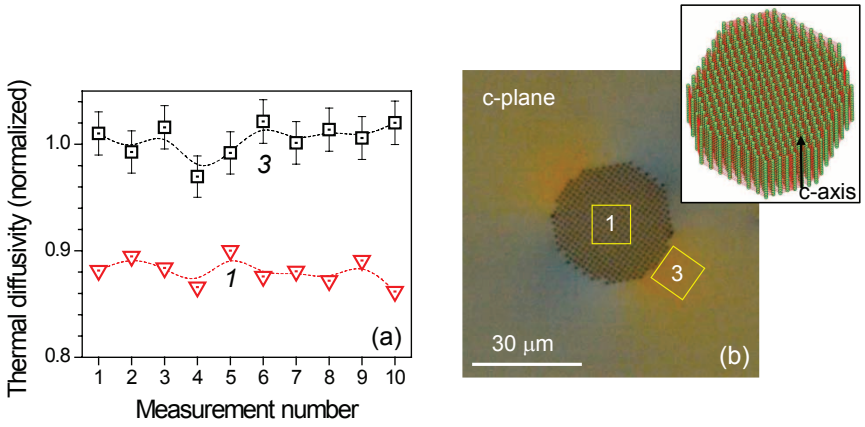


Fig. 2. (a) Normalized thermal diffusivity, $\chi_S/\chi_{host}$, (see, Fig. 1(b)) through the laser-structured (*1*), adjacent (*3*) regions vs number of measurement cycles. Error bars are 2%. (b) Polariscope image shows a region laser-structured by 80 nJ/pulse energy with two pulse per irradiation site. An approximate location and size of the hot-junction sensors are marked. Inset shows a slanted view of the computer generated 3D pattern of the irradiation spots (circles) and the movement path (lines).

smaller than $\Lambda$, which is typically several tens of nanometers, scattering increases, and $\tau$ is reduced, causing smaller $\Lambda$ and $k_c$. Because of these effects, objects with nanoscale-volumes can efficiently localize heat as was demonstrated by polymerization [29]. Such a large 12% modification of thermal property on the scale of several micrometers can be used for the temperature localization at required location which can be freely three-dimensionally recorded inside bulk of transparent host crystal.

The same thermal analysis has been carried out for BK7 glass and the thermal diffusivity value of $(4.81 \pm 0.027) \times 10^{-7}$ m$^2$/s (at 45°C) has been determined for the host matrix as expected [30]. A reduction of thermal diffusivity up to 2% in the fs-laser structured regions is observed which is considerably less than in crystalline sapphire. Since BK7 is amorphous the decrease of thermal conductivity might be caused by structural changes in ring-like structures of $SiO_4$ tetrahedrons which occur due to densification of glasses [8, 18, 31].

### *3.2. Birefringence and azimuthal phase*

The stress-induced birefringence was measured by polariscopy using a phase compensation technique for the changes caused by stress-induced birefringence [22]. The intensity of the transmitted light through an optically-crossed polarizer and analyzer with a birefringent material in between is given by [32]:

$$I_t(\varphi, \Delta n) = I_0 \sin^2(2\varphi) \sin^2(\Gamma/2) \tag{3}$$

where $\varphi$ is the angle of the polarizer axis with the principal stress direction in the sample, $\Delta n$ is the induced birefringence, $d$ is the axial extension of the region, and $\lambda_0$ is the wavelength of light in vacuum, and $\Gamma/2 = \pi \Delta n d/\lambda_0$ is the retardance. Equation 3 represents the well known Maltese cross intensity distribution (illustrated in the inset of Fig. 1(b)), where the principle directions of stress coincide with the dark lines and points ($\varphi = 0$), called isoclinic, in the polarization micrograph. The brightest regions are at $\varphi = \pi/4$ angles. By performing Stokes analysis the birefringence, $\Delta n$, and the azimuth, $\Psi$, or the angular distribution of an optical slow

#123699 - $15.00 USD Received 2 Feb 2010; revised 26 Mar 2010; accepted 29 Mar 2010; published 6 Apr 2010

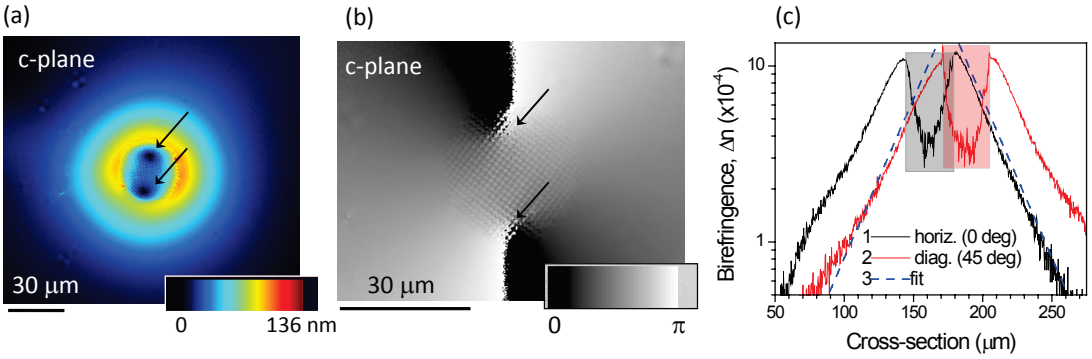


Fig. 3. Polariscopy data. (a) The amplitude, i.e., retardance distribution $\left(\frac{\Gamma(x,y)/2}{\pi}\times\lambda_0\right)$ [nm] on a c-plane of sapphire sample with a fs-laser structured region of 30 $\mu$m in diameter at the center (as shown in Fig. 2(b)). (b) The azimuth or distribution of the slow axis orientation, $\Psi(x,y)$. The arrows are pointing to location of a pair of topological phase defects where birefringence and the orientation of the polarization ellipsis are undefined. Scale, radians. (c) Horizontal and diagonal cross-sections of the birefringence, $\Delta n(x,y)$, map given in (a); calculated from experimentally measured retardance $\Gamma(x,y)/2=\frac{\pi}{\lambda_0}\Delta n(x,y)d$ ($\lambda_0=546$ nm, $d\simeq 90$ $\mu$m). The exponential $1/e$ fits with a birefringence (stress) relaxation constant $\tau_R=24$ $\mu$m are shown as eye guides. Red and grey marked regions indicate the laser structured locations. Pulse energy was 80 nJ/pulse. Stress-induced crack formation is demonstrated at the corners of volume with a square footprint (Media 1); this proves a stress-related origin of the birefringence rather than form-birefringence.

axis can be retrieved for the each pixel of a microscope image, e.g., the Stokes parameter $s_3$ is related to the retardance via $s_3=-\cos\Gamma$ [33].

Results of the imaging polariscopy analysis are summarized in Fig. 3 for the amplitude (a) and azimuth (b). The amplitude is the retardance presented in nanometers $\left(\frac{\Gamma(x,y)/2}{\pi}\times\lambda_0\right)$ [nm] and the azimuth shows slow axis orientation [22].

First, we discuss modifications observed outside the cylindrical fs-laser structured regions (see, Fig. 2(b)). The birefringence with maximum of $\Delta n\simeq 1\times 10^{-3}$ is determined before onset of micro-crack formation for the laser-structured volume used in our experiments. The typical distance over which the birefringence (and stress) relaxed single-exponentially was $\tau_R=24$ $\mu$m (c). The slow axis orientation, the azimuth [22], has radially and azimuthally varying distribution shown by dial-markers in more details in Fig. 4. The azimuthal phase retardation over one full turn around the cylindrical laser structured region of 90 $\mu$m length and 30 $\mu$m diameter was $\sim 2\pi$ as revealed by two gradient lobes with a change over $\pi$ each. Hence, a light waveguided around such laser structured volume in the region of high birefringence would acquire an orbital angular momentum. By recording cylindrical structure inside sapphire the local orientation of optical axis and birefringence can be controlled.

The polariscopic analysis inside the laser structured volume is only qualitative for birefringence since a strong light scattering, as observed in earlier Raman studies [34], causes depolarization of light (boxed regions in Fig. 3(c)). Stress-induced birefringence can be measured with few micron resolution using polariscopy [31]. The two dark regions inside the laser structured volume marked by arrows in Fig. 3 represent topological defects where the orientation of polarization ellipsis is undefined or has a singularity [35] (also, marked in Fig. 4). The location of

#123699 - $15.00 USD Received 2 Feb 2010; revised 26 Mar 2010; accepted 29 Mar 2010; published 6 Apr 2010

the phase defects is related to the stress distribution, which is defined by the crystalline orientation of the sample, its thickness, geometry of the recorded pattern, and most probably to the shape of voids and amorphous regions (see Media 1 online file for details). Such singularities are common in different fields of physics and optics [36–40], e.g., pipe-dislocations in GaN crystals [41] and disclinations in liquid crystal films [42]. The disclinations of the director in liquid crystals equivalent to the orientation shown in Fig. 4(b) are defined by the strength parameter $s = +1/2$. The azimuth of optical axis around each of two singularity points (Fig. 4(b)) is increasing anti-clockwise and in a full turn acquires a cumulative $\pi$ phase change.

The stress-induced birefringence can be used to generate optical vortex [43] as demonstrated for the macroscopic stressed glass waveplate. The optical vortex is characterized by the azimuthal phase which is changing as $\exp(il\psi)$, where $\psi$ is the local azimuthal angle and $l$ is an integer number, the topological charge. The laser-structured volumes create birefringence and a smooth continuous change of azimuthal orientation of the optical axis, hence, such structure would generate optical vortex from a micro-volume in contrast to a large optical element [43]. Alternatively, the micro-optical elements with space-varying birefringence can be recorded in an optically isotropic micro-volume of sapphire (or other material) and the micro-workpiece can then be released by wet-etching [25] for laser trapping applications. Once a micro-particle has birefringence and refractive index is larger than that of surrounding, it can be laser-trapped and spined [44–46], thus, performing pump, sorting, or other mechanical functions in optofluidic applications.

Since the charge, $l$, of an optical vortex is related to a particular 3D geometry of a spatially-variant birefringence and readout beam (a focusing angle) [47, 48], one would expect that by choosing other shapes of laser-structured micro-volumes one could obtain singularities of different topological charges. At the singularity location a minimum of light intensity is obtained and it is well localized. This has number of potential applications in physics and optics [36–40, 49].

We have chosen to record structure by laser structuring along c-axis, the direction for which sapphire has no birefringence, and to explore stress-induced birefringence and its spatial and azimuthal distribution. Crystal parameters such as photoelastic constants (discussed in next section) related to the Stokes parameters and the bulk modulus govern a birefringence change, its azimuthal distribution, handedness, and optical activity. It would be necessary to explore next, how by changing particular micro-pattern recorded inside bulk of crystal or glass, one could tailor the required changes of birefringence, handedness, optical activity using direct femtosecond laser writing. Such patterns could be used to form vortex beams which carry an orbital angular momentum due to stress-induced spatially variant birefringence around or inside regions specially tailored by laser fabrication. It might have applications in optofluidics, design of micro-optical elements, and laser trapping [50, 51].

### *3.3. Determination of stress*

Let us determine the stress responsible for birefringence of $\Delta n \simeq 10^{-3}$. The refractive index of a crystal is related to stress, $\sigma$, through the stress-optic (piezo-optic) tensor $q_{ij}$ or to strain through the strain-optic (elasto-optic or photoelastic) tensor $p_{ij}$; in the Voigt nomenclature elements of tensors are interrelated $p_{ij} = q_{ij}c_{ij}$ with $c_{ij}$ being the stiffness tensor [52]. Strain ($\varepsilon$) is related to stress ($\sigma$) through the compliance tensor, $s_{ij}$, and vice versa. The Hook's law defines a stress-to-strain relation via stiffness $\sigma_i = c_{ij}\varepsilon_j$ [53].

The stress-induced birefringence $\Delta n = n_{\parallel} - n_{\perp} \simeq \frac{n_0^3}{2} q\sigma$ where $n_0$ is the average refractive index, $n_{\parallel}$ and $n_{\perp}$ are the refractive indices for light with its electric vector parallel and perpendicular to the direction of stress, respectively. The $p_{ij}$ [54, 55] and $c_{ij}$ [56] values of sapphire were used for calculation of the stress-induced birefringence. In the employed imaging geom-

#123699 - $15.00 USD Received 2 Feb 2010; revised 26 Mar 2010; accepted 29 Mar 2010; published 6 Apr 2010

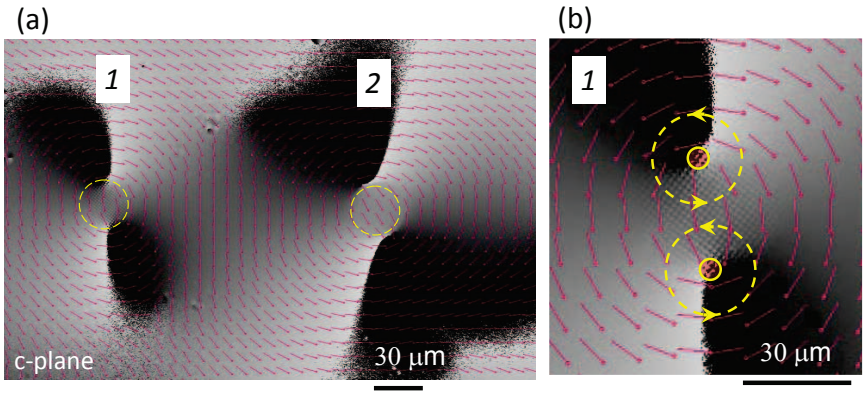


Fig. 4. (a) The azimuth, $\Psi(x,y)$, (grey scale map $0-\pi$) map around two regions of smaller $\Delta n_{max} \simeq 10^{-3}$) *(1)* and by 50% larger *(2)* birefringence; the dial-markers shows the orientation of the azimuth; pulse energies were 80 *(1)* and 120 nJ/pulse *(2)*, respectively. The central laser structured regions have the same 30 $\mu$m diameters (marked by circles). (b) Close up view of the central part of region *(1)* with two singularities of azimuthal orientation of the polarization ellipsis. A round trip phase changes by $\pi$ for the two singularities (marked by arrows).

etry along c-axis (Fig. 1(b)) the stress component, $\sigma_3$, can be estimated assuming transversely isotropic conditions with symmetry axis along $\mathbf{e}_3$ as $\sigma_3 = c_{13}\varepsilon_1 + c_{13}\varepsilon_2 + c_{33}\varepsilon_3 \simeq (2c_{13} + c_{33})\varepsilon$. We used sapphire constants $c_{13} = 117.2$ GPa, $c_{33} = 501.8$ GPa [56], $p_{13} = 0.005$, $p_{33} = 0.23$ [55] for evaluation of effective coefficient $q_{33}$. It is noteworthy that when the recorded pattern inside sapphire exert a complex 3D stress pattern this proposed estimation can only be used for a qualitative measure since the model is valid for the patterns which are 2D and when their cross sections are considerably larger than the wavelength of light. One would find that a $\sigma_3 = 2\Delta n/(n_0^3 q_{33}) \simeq 125$ MPa stress is required for the $\Delta n = 1 \times 10^{-4}$ birefringence when an average refractive is $n_0 = 1.7$. This is one of the highest photoelastic sensitivities among crystals which is caused by the high $p_{33}/p_{13}$ ratio as first reported in ref. [57]: an experimentally validated value of $\Delta n = 1 \times 10^{-4}$ birefringence was obtained for the 1 kbar (0.1 GPa) hydrostatic pressure.

The experimentally measured birefringence of $10^{-3}$ corresponds to the stress of $\sim 1.3$ GPa for the employed geometry of laser structuring along c-axis. Since sapphire has the Young modulus of 400 GPa, pressures up to 1 GPa can be created by fs-laser structuring without crack formation [58] and can be used for waveguiding.

## 4. Conclusions

It has been established that the thermal diffusivity of fs-laser structured micro-volumes in sapphire is reduced by 12% as compared with the host crystalline matrix. Such large change of thermal property can be localized with several micrometers precision inside the bulk of crystalline host. Due to high crack propagation resistance [58] (mainly determined by a high value of Young modulus $\sim 400$ GPa) the crack-free regions of birefringence up to $\Delta n \simeq 1 \times 10^{-3}$ can be formed adjacent to the laser-structured volume and spanning tens of microns. This opens a possibility to form 3D waveguides inside sapphire, ruby (Cr-doped sapphire [59]), and other laser crystals which have comparable mechanical properties and can be used for formation of active lasing waveguiding structures. Thermal diffusivity in the stress-birefringent regions was

#123699 - $15.00 USD Received 2 Feb 2010; revised 26 Mar 2010; accepted 29 Mar 2010; published 6 Apr 2010

found unchanged.

Polariscopy imaging is used to quantify the stress-induced birefringence around laser-structured volumes. The peak birefringence of $\Delta n \simeq 10^{-3}$ at the edge of laser structured volume is decaying exponentially with spatial constant $\tau_r = 24$ $\mu$m. It is found that azimuth of slow axis is spinning around the laser structured region. This opens possibility to engineer and tailor optical activity and record functional polarization-sensitive micro-devices, e.g., for generating optical vortex beams.

The quantitative measurement of birefringence is used to estimate the stress. The cylindrical volume composed of void-structures exerted a 2D stress pattern. This simplified calculations and the following correspondence has been established: $\Delta n \simeq 10^{-3}$ is equivalent to 1.3 GPa stress.

Presented combined assessment of optical, mechanical, and thermal properties inside and around laser structured regions in sapphire should help for miniaturization of optically active and passive functional micro-devices, polarization micro-optics, and can be applied to other crystalline materials and glasses.

## Acknowledgments

Support via a Discovery ARC Grant DP0988054, Grant-in-Aid from the Ministry of Education, Science, Sports, and Culture of Japan No. 19360322, and a grant from Japan Science and Technology Agency (Development of System and Technology for Advanced Measurement and Analysis) are gratefully acknowledged. Authors would like to thank Etienne Brasselet for useful discussions, and Tokyo Instruments, Inc. for agreement to publish data obtained by Abrio IM microscope.

#123699 - $15.00 USD Received 2 Feb 2010; revised 26 Mar 2010; accepted 29 Mar 2010; published 6 Apr 2010